Modeling Fuel Droplets in RCS Engine Exhaust Plume

Camila B. Cabrera

OSTEM Summer Intern

Deep Space Logistics

Kennedy Space Center

Internship Mentor: Dr. Jonathan S. Pitt

July 7, 2023

Abstract

Thrusters are used to maneuver spacecraft in space. Spacecraft maneuvering and attitude control is achieved by accelerating the high temperature and pressure exhaust gases, which are the result of chemical combustion in the case of chemical engines, through the rocket nozzle. Following the end of the nozzle a plume is created containing combustion gases and high velocity droplets of unburnt propellant that with time can erode the surfaces it strikes. A simulation that can accurately model a thruster's plume can help us reduce the erosion of components struck by the plume. The creation of this simulation can be broken into several parts, and this paper focuses on finding out what distribution of particles along a plane in the nozzle, where combustion can be assumed to be complete, creates the observed particle distribution in the plume. Findings show that unburnt droplets are mostly concentrated in the center of the nozzle or uniformly dispersed within the nozzle.

Table of Contents

1. Background Information

Reaction Control System (RCS) thrusters are used in space operations to maneuver spacecrafts before docking them to a station or to reposition satellites back into their orbits. The firing of these thrusters creates a downstream jet flow from the nozzle called a plume [1, 2]. Although the plume is mostly made up of combustion gases from the hypergolic combustion it contains small droplets of unburnt fuel that solidify as they enter the low temperatures of space.

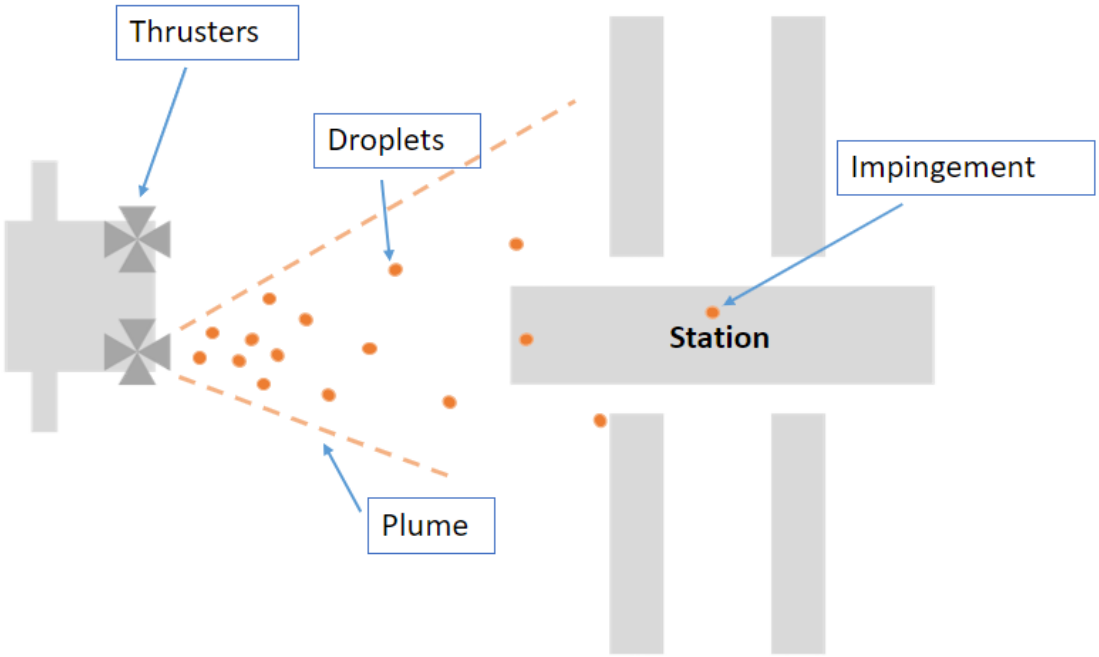

Figure 1. Plume impingement

As particles exit the nozzle, they convert significant amounts of thermal energy into kinetic energy, giving them a high velocity. The plume flow can interact with surrounding objects, as show in figure 1, and cause undesired effects such as unexpected forces, heat loads, and contamination which can create erosion and reduce the lifetime of the impacted objects [1]. Understanding and creating a plume model for every station and visiting vehicle thruster can help us reduce the undesired impartation of forces, heating, contamination, and erosion of components.

In the vacuum of space, the plume expands to a maximum to the point where the flow can no longer be represented as a continuum flow [2]. For a Knudsen number (Kn) less than 0.01 the

flow can still be described as a continuum and can therefore be simulated through the application of traditional computation fluid dynamics (CFD) however for Kn>0.01 where the flow is transitioning to rarefied regime a discrete simulation Monte Carlo (DSMC) method needs to be used. This transition from continuum to rarefied flow is a key issue when modeling an RCS plume expanding into a space environment. Simulating this sort of plume structure requires the development of a hybrid CFD-DSMC model. As a preliminary step, the scope of this work aims to understand the flow through the rocket engine nozzle and immediately downstream of the nozzle where the Kn<0.01. We are investigating how the underlying physics affects the density distribution of particles as transition from continuous to rarefied flow field.

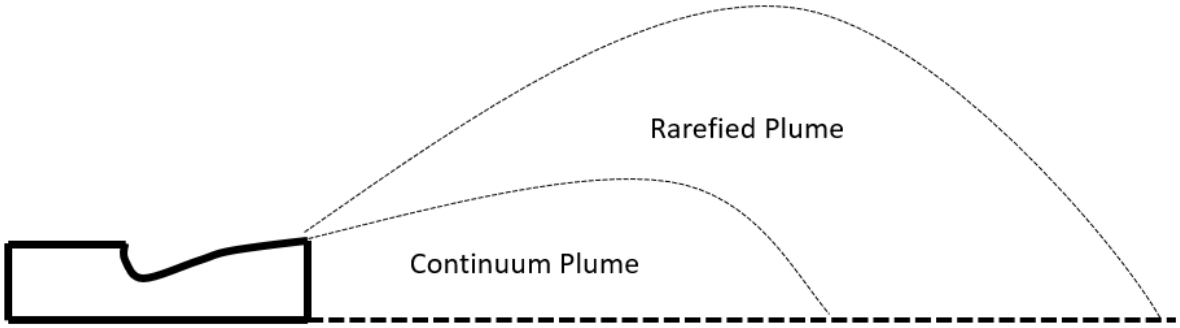

Figure 2. division between continuum and rarefied regime in plume

2. Methodology

The final CFD model will include multiphase effects including unburnt fuel droplets and/or particles; however, because its development is complex it requires breaking it up into smaller component as seen on Table 1.

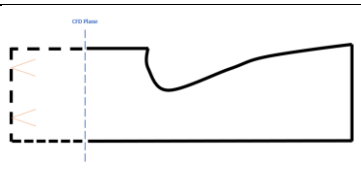	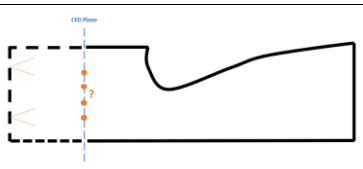	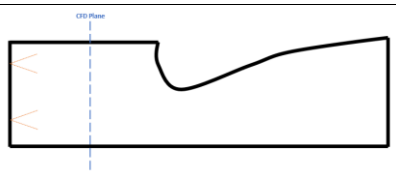
1.Turbulent gas flow after combustion, this is a non reactive flow. Simulation starts at CFD plane.	2. Particle distribution of CFD plane, this helps locate where the concentration of most unburnt droplets can be found	3. Multiphase, turbulent combustion and droplet formation. This simulation begins at the beginning of nozzle

Table 1. Breakdown of CFD model

The development of the physics through the nozzle and within the continuum regime of the plume that governs the non-reactive gaseous flow was created by a previous intern, part 1 on Table 1.

The next component, part 2 in Table 1, is the incorporation of Lagrangian particles into the current non-reactive simulation and finding out what distribution of particles along the CFD plane creates the observed particle distribution in the plume, this is the first component of this internship.

The following assumptions were made for the simulation

1. Multiphase combustion is largely complete, justifying the simplification of a non-reactive gas flow
2. Droplet distribution is smooth radially and uniform angularly due to turbulent mixing
3. Simulation is axisymmetric and we use a prescribed particle flow rate
4. Droplets do not interact with each other, and they are perfect spheres with a constant size

2.1 Empirical Model

Initially, it is important to understand the behavior of unburnt droplets in the plume. Previous studies by Larin [3] [4] [5] have led to the development of two equations quantifying physics in the plume, one for the droplet number flux, $\dot{n_d}$, and the other for the droplet velocity V [3].

$$\dot{n_d}(T,r,\theta,d) = \frac{k \cdot \dot{M_T} \cdot T^{-\beta}}{S_m} \cdot (r + l_{noz})^{-2} \cdot \left(\frac{d}{d_{min}}\right)^{-p} \cdot e^{\frac{-\theta^2}{2\sigma^2}} \quad \left[\frac{\#\ of\ particles}{cm^2 \cdot s}\right] \tag{1}$$

$$V(T,d,\theta) = \left(0.7e^{-0.015*\left(\frac{d}{d_{min}}\right)^{1.19}} + 0.3\right) * \left(0.0277 * \ln\left(\frac{T}{T_{min}}\right) + 0.06811\right) * U_{lim} \tag{2}$$

Where:

K=curve fit coefficient

$\dot{M_T}$=Propellant Flow rate

T=Thrust

β=Slope of curve fit for initial deposit

S_m=conversion factor from mass flux to number flux

r = distance from Nozzle edge to particles in plume

l_{noz}=nozzle length

d =droplet diameter

d_{min}=minimum droplet diameter

θ = angle between centerline and particle in plume

σ=a function of the limiting angle

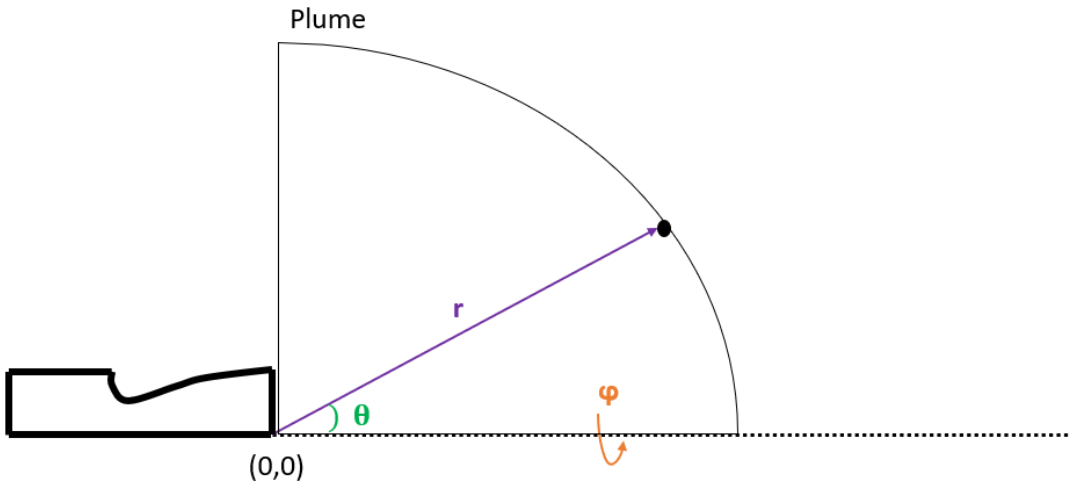

Figure 3 Coordinate system for plume

These equations will be used as validation data for the CDF results generated during this research for example the number droplet flux from the simulation should match the trends outlined by the Larin equations.

From equation 1 it is expected that given a constant thrust, particle diameter, and radial distance from the nozzle exit center, r, as shown in figure 3, the droplet number flux as a function of theta will follow a gaussian trend.

2.2 Recreation of graphs

Alred [6] used Equation's 1 and 2 to explain the effect particle size has on the number density and velocity of droplets in the plume. The graphs created by Alred [6] are being re-created by us, for the Primary Reaction Control System (PRCS) of the Space Shuttle, to assure that the equations are properly coded. Once all three graphs match, the input parameters will be changed to those of the R-4D-11 490N thruster. This will allow us to validate the CFD simulation for the R-4D-11 490N thruster by comparing the results of the simulation with those from the empirical model.

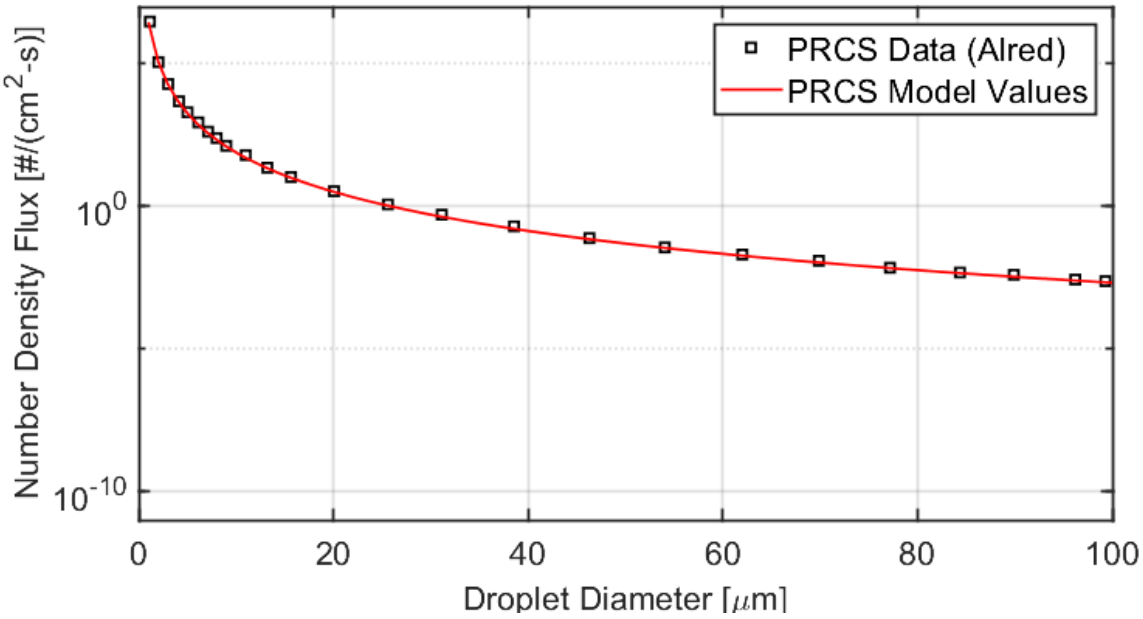

Figure 4 Comparison between Number density flux vs droplet diameter in Alred paper and model using Larin equation. Both plots agree closely on the trend that as particle size increases the number density decreases at the centerline

```
%Camila Cabrera_OSTEM Intern 2023
%Number Densiy vs Particle Diameter for Orbiter Vehicle


%Constants
K=0.5258 ; %curve fit coefficient for initial deposit from Soares 2001
B=0.4816 ; %slope of curve fit for initial deposit from Soares 2001
S_m= 1.18*10^(-12)/1000; %Conversion factor from mass flux to number flux, grams, from Soares 2015
r= 20*100; %distance from nozzle, m, Alfred 2003
d_min= 1; %minimum droplet diameter size, micrometer
p= 4.57; %Droplet size distribution parameter updated, from Soares 2015
theta= 0; %only for centerline particles


%ISS Thruster Specification (currently for Orbiter), source: Soares 2001
T=3870 ; % Thrsut, N
Isp=280 ; %Specific Impulse, s
M_T=T/(Isp*9.81) %Propellant flow rate, kg/s
L_noz=236.22/10 ; %Nozzle length, mm

%data vectors
d=linspace(1,100,100); % particle diameter
n=(K*M_T*T^(-B))/S_m*((r+L_noz)^(-2))*(d/d_min).^-p %Number density equation


%plot
semilogy(d,n)
title('Number Density Comparison')
xlabel('Particle Diameter (um)')
ylabel('Number Density (#/cm^2-sec)')
```

Figure 5 Cabrera code for Number Density Flux vs Droplet Diameter

From figure 4 above it is clear that along the centerline most of the particles will have a diameter between 1 and 20 µm.

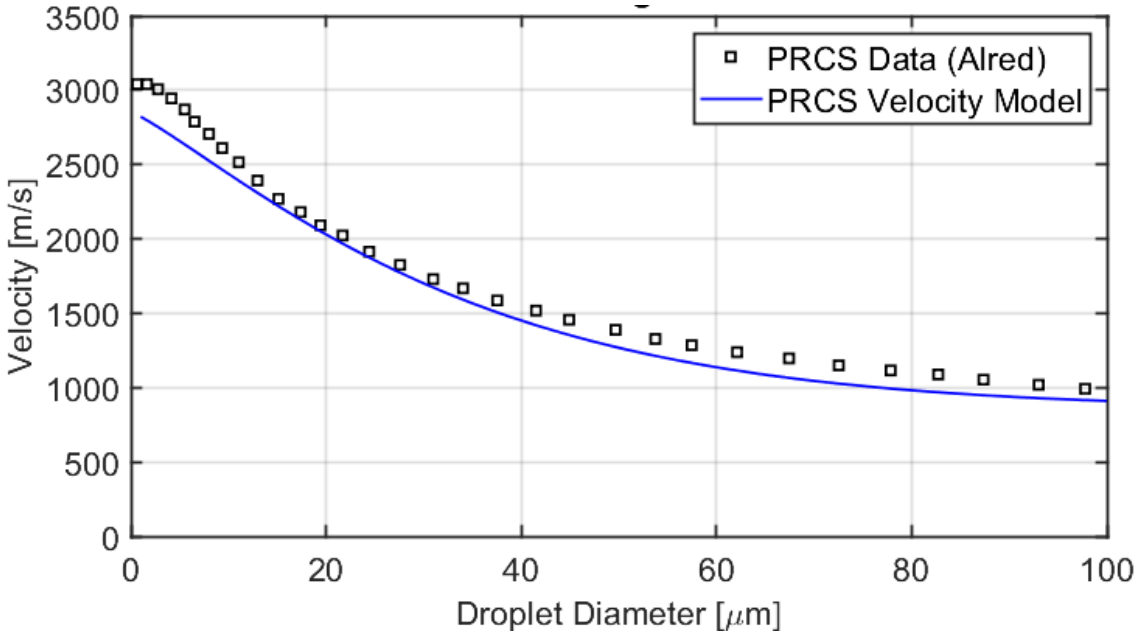

Figure 6 Comparison of droplet velocity variation with droplet size along the centerline in Alred paper and model using Larin equation. Both plots display a similar trend that smaller particles will have a significantly higher velocity than their larger counterparts

```
%Camila Cabrera_OSTEM Intern 2023
%Velocity vs Diameter for Orbiter Vehicle


%Constants
d_min= 1; %minimum droplet diameter size, micrometer
T_min=1; %Minimum Thrust Level, depends on the study, N, Larin 2001

%ISS Thruster Specification (currently for Orbiter), source: Soares 2001
T=3870 ; % Thrsut, N
Isp=280 ; %Specific Impulse, s

%Calculated variables
U_lim=Isp*9.81 %limiting velocity, m/s

%data vectors
d=linspace(1,100,100); % particle diameter
v= (0.7*exp(-0.015*(d/d_min).^1.19)+0.3)*(0.0277*log(T/T_min)+0.6811)*U_lim %drop velocities

%plots
plot(d,v)
title('Velocity vs Droplet Diameter')
xlabel('Droplet Diameter (um)')
ylabel('Velocity (m/s)')
grid on
```

Figure 7 Cabrera Code for Droplet velocity variation with droplet size on the axis

Using the information from figure 4 and 6, particles exiting PRCS thrusters, located near the centerline of the plume will most likely be under 20 µm in diameter but traveling at extremely high velocities between 2,000 and 3,000 m/s.

Finally, the number density vs droplet size for different angles was re-graphed using Octave.

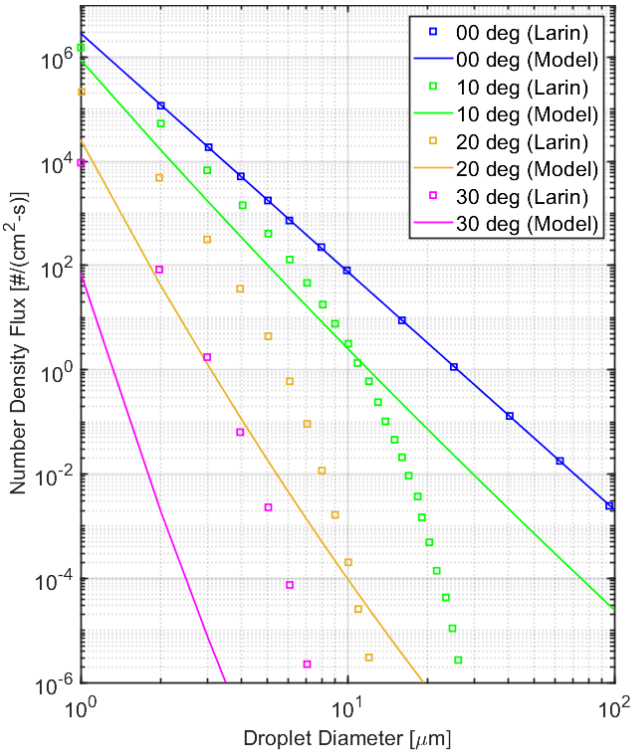

Figure 8 Comparison of droplet distribution in Alred paper and model using Larin equation.

Although the results from the Alread paper and the model replicated in this research differ in Figure 8, both clearly show that the bigger the particle the closer they tend to stay near the centerline. The discrepancy in the plot's behavior is currently being studied, it is predicted that the equation used in the Alred paper has a modification most likely with the equation used to calculate the value of σ as a function of the limiting angle and droplet diameter. Unfortunately, the exact relationship used by Alred was not given in his paper. My mentor has reached out to the co-authors at Johnson Space Center for clarification, and when received, we will incorporate that into this work.

2.3 Finding the droplet concentration

The next step is to figure out where the concentration of unburnt particles is in the nozzle that produces the observed trends for number density from the Larin equation in the plume. The data from observed number density in the Larin paper will validate what distribution of particles in the CFD simulation is the most likely.

The total number of particles per second entering through the nozzle inlet must be the same as the total number of particles at a distance **r** from the nozzle, therefore,

$$\dot{N}_0 = \int_0^{2\pi} \int_0^{\frac{\pi}{2}} \dot{n_d}(T, r, \theta, d) d\theta d\varphi \tag{3}$$

Which can be simplified to...

$$\dot{N}_0 = 2\pi \int_0^{\frac{\pi}{2}} \dot{n_d}(T, r, \theta, d) d\theta \tag{4}$$

Were $\dot{N}_0$ is the total number of particles per second entering the system and $\dot{n_d}(T, r, \theta, d)$, the number density flux, comes from the Larin paper.

We can fix the T, r, and d values in this equation and leave it only as a variable of θ and solve for $\dot{N}_0$. We can choose a $\dot{N}_0$ for a given diameter, d, while the discrepancy in the Larin number density flux equation is being studied and use a correction factor later to scale it.

For a uniform initial distribution along the CFD plane in the nozzle, the number density flux equation can be expressed as

$$\dot{n} = D \tag{5}$$

where $\dot{n}$ is the number density flux and D is a constant

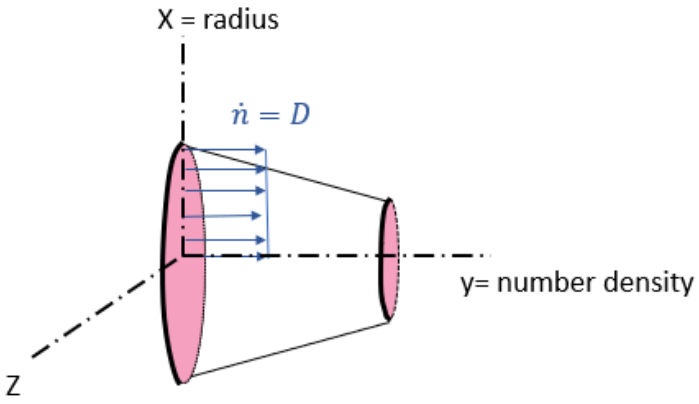

Figure 9 Visualization of uniform number density flux equation

To find the total number of particles per second, the following equation can be used

$$\dot{N}_0 = \int_0^D \pi R^2 dy \tag{6}$$

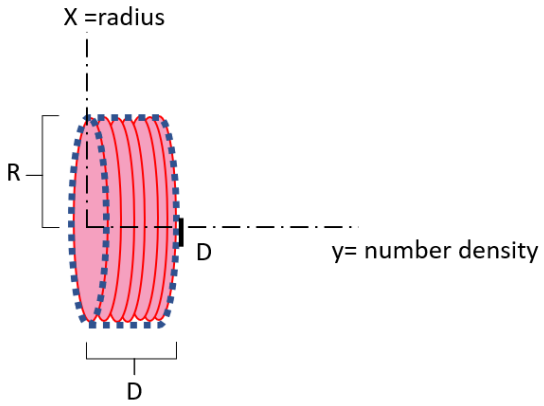

Figure 10 Visualization of total number of particles per second for uniform case

The number of droplets per second, $\dot{N}_0$, at a distance r from the plume must be equal to the number of droplets per second at the nozzle inlet therefore:

$$\dot{N}_0 = \int_0^D \pi R^2 dy = 2\pi \int_0^{\frac{\pi}{2}} \dot{n}_d(T, r, \theta, d) d\theta \tag{7}$$

It is now possible to solve for constant D

$$D = \frac{2\pi \int_0^{\frac{\pi}{2}} \dot{n}_d(T, r, \theta, d) d\theta}{\pi R^2} \tag{8}$$

For the gaussian distribution the equation for the number density is as follows:

$$\dot{n} = Ae^{-\frac{(-r-\frac{R}{2})}{\mu^2}} \tag{9}$$

Where A is an unknown constant and μ=1

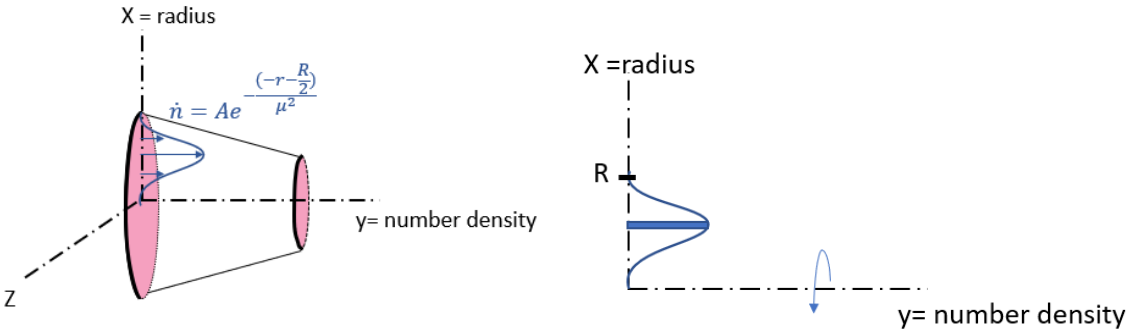

Figure 11 Visualization of Gaussian particles per second equation

The number of particles per second can be written as follows…

$$\dot{N}_0 = 2\pi \int_0^R r * (Ae^{-\frac{(r-\frac{R}{2})^2}{\mu^2}}) \mathrm{dr} \tag{10}$$

Because the particle flow rate stays constant for all distributions it is possible to find A

$$A = \frac{\dot{N}_0}{2\pi \int_0^R r * (e^{-\frac{(r-\frac{R}{2})^2}{\mu^2}}) \mathrm{dr}} \tag{11}$$

By finding the constants, A and D, in these particle flow rate equations, it is possible to calculate the number density in the nozzle. This approach is still under development pending further

discussions with the model developers, and a simplified approach was taken in the subsequent sections.

3. Analysis

Because the main interest is to find a general distribution for where the unburnt droplets are located within the nozzle that results in the empirical equation for droplet number flux in the plume model derived by Larin [3], four cases were developed for possible particle concentrations: constant/uniform, center, middle, and wall distributions, illustrated in figure 12. These regions were then uniformly divided into 5 sections and an injector was placed in each for a total of 5 droplet injection points.

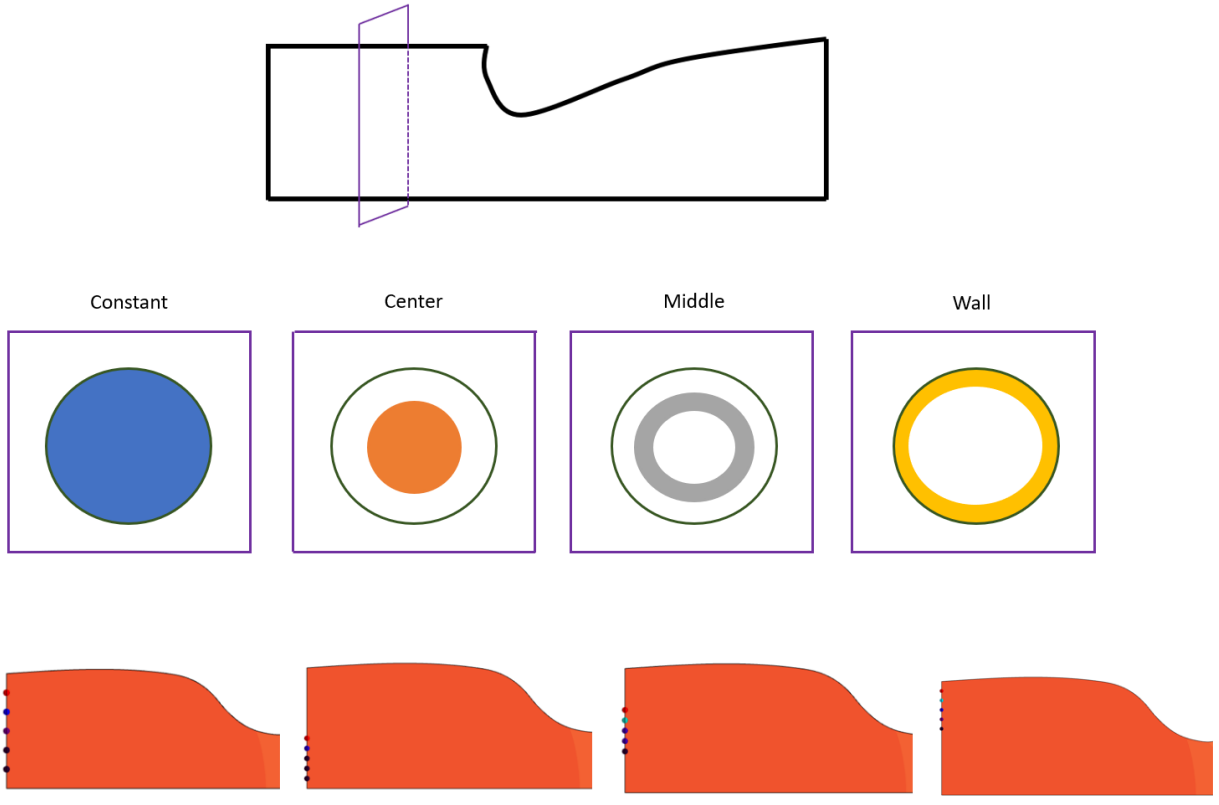

Figure 12 Particle concentration

The Star CCM+ simulation was then run for each case and the angle θ, see coordinate system in figure 3 for reference, for the particles at the end of the plume was recorded as shown on figure 16.

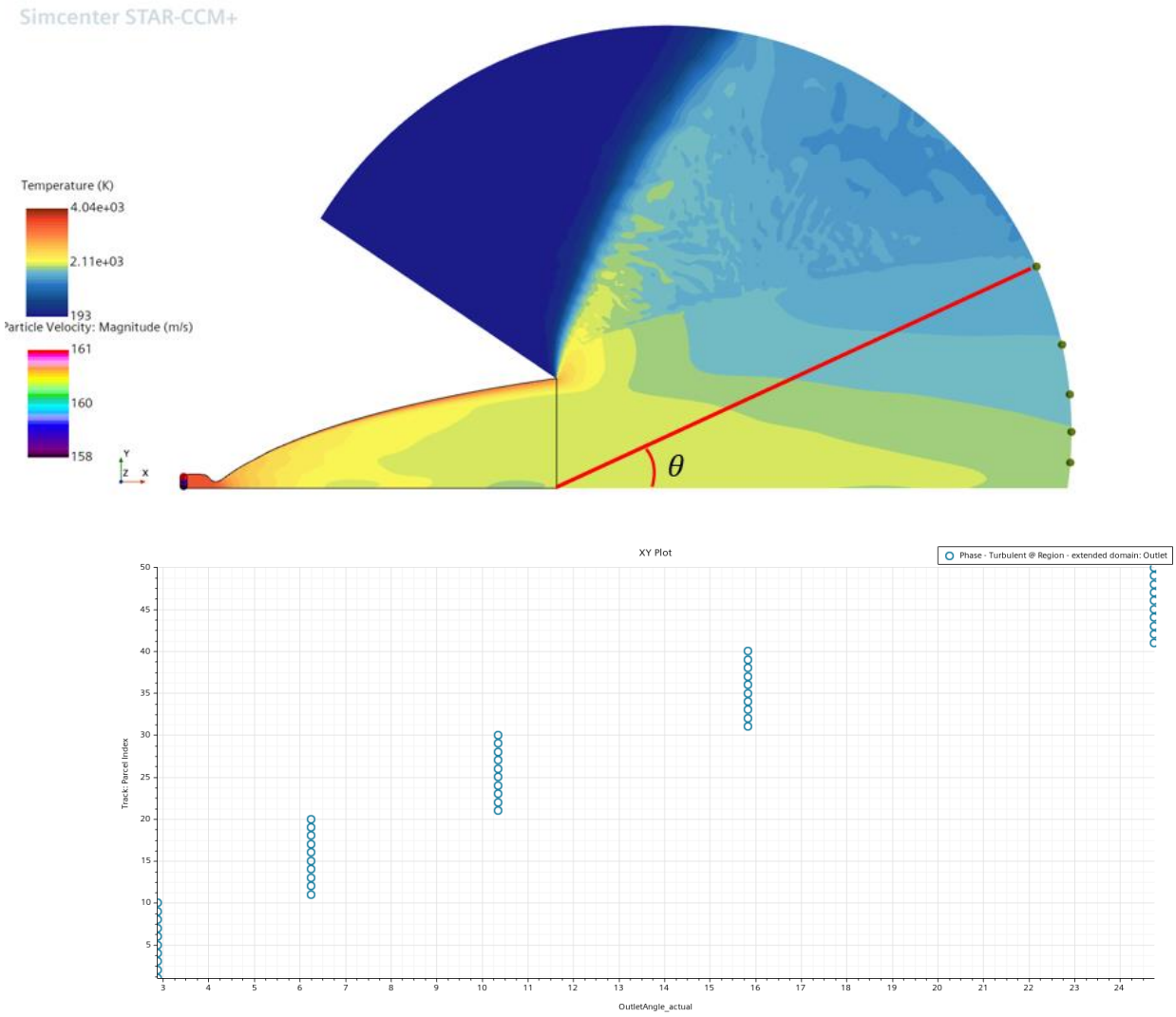

Figure 13 Angle calculation on StarCCM+

Because number density is the number of particles per unit area every second, an equation for the surface area of the cap, A_s , in terms of the angle and radius was derived.

$$A_s = 2\pi r(r - \cos(\theta) * r) \qquad (12)$$

This formula gives the surface area of the spherical cap that encompasses the particles. Caclulations for each of the 4 cases in figure 12 were performed and the resulting graph in figure 14 contains for a given diameter size of 1µm the normalized number density at different angles.

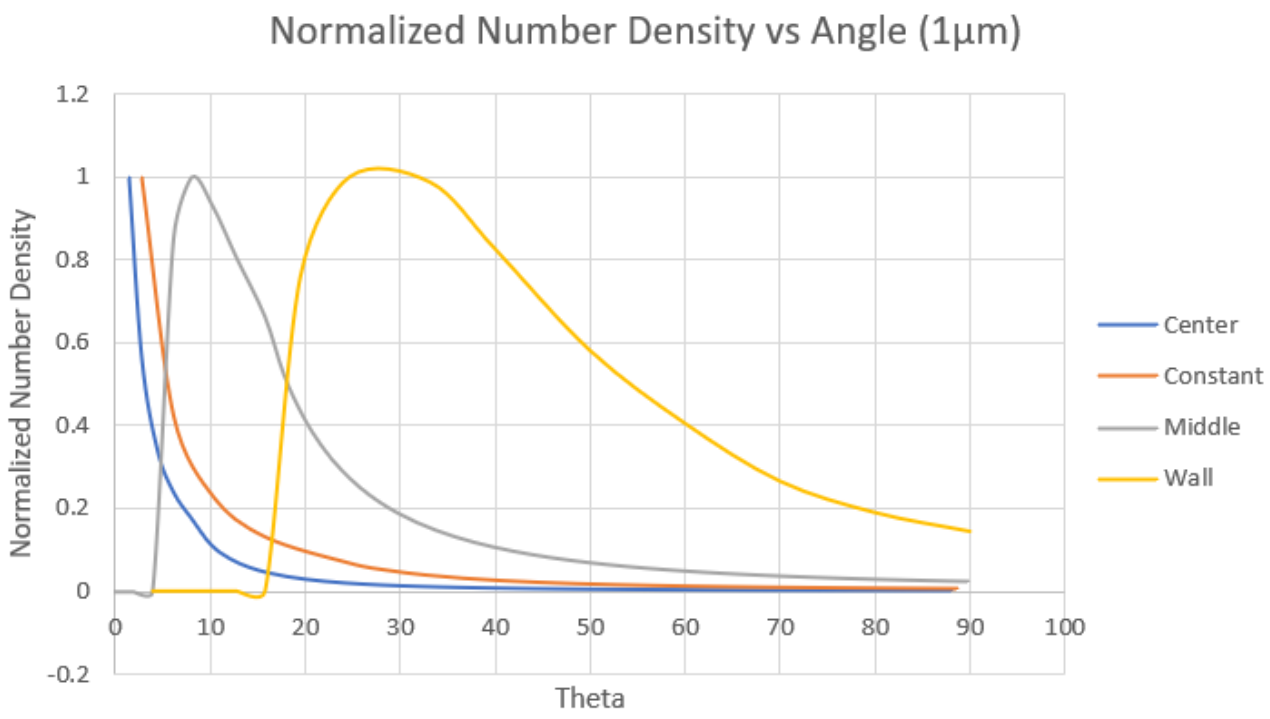

Figure 14 Normalized Number density vs angle for the 4 distribution cases.

All four cases follow a gaussian trend as expected from the Larin equation for number density. The center and constant distributions have a higher particle concentration near the centerline, which agrees with the Larin equation for number density flux as the gaussian is centered at 0. The middle distribution has a number density flux centered at 10 degrees and the wall distribution has a number density flux centered at 30 degrees range making both unlikely representations of the actual concentration of unburnt droplets in the nozzle.

A similar procedure to the one described above was followed to find the number density and angle for the 100µm particles, which are the max extreme of possible particle diameters. And the results were compared to those of the 1µm particles.

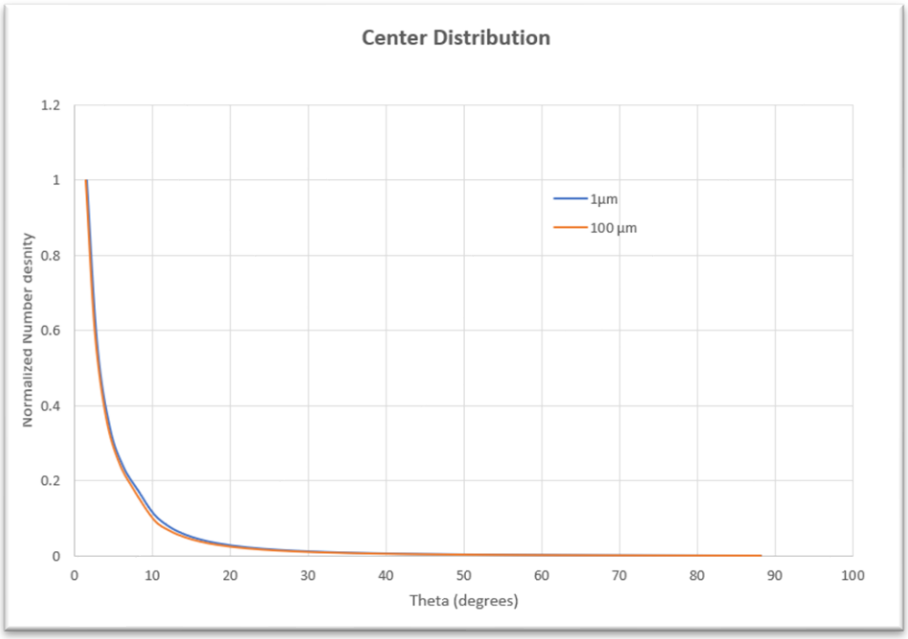

Figure 15: Number density vs angle comparison between 1µm and 100µm diameter particles for the center distribution case. The 100µm diameter droplets are found slightly closer to the centerline than their 1µm counterparts originating from the same location within the nozzle.

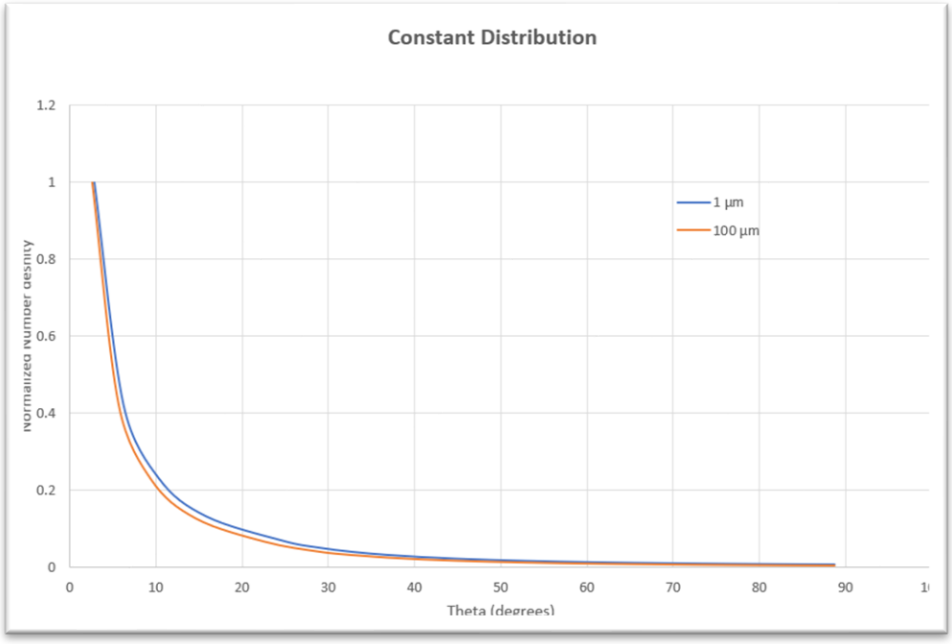

Figure 16: Number density vs angle comparison between 1µm and 100µm diameter particles for the constant distribution case. The 100µm diameter droplets are found slightly closer to the centerline than their 1µm counterparts originating from the same location within the nozzle.

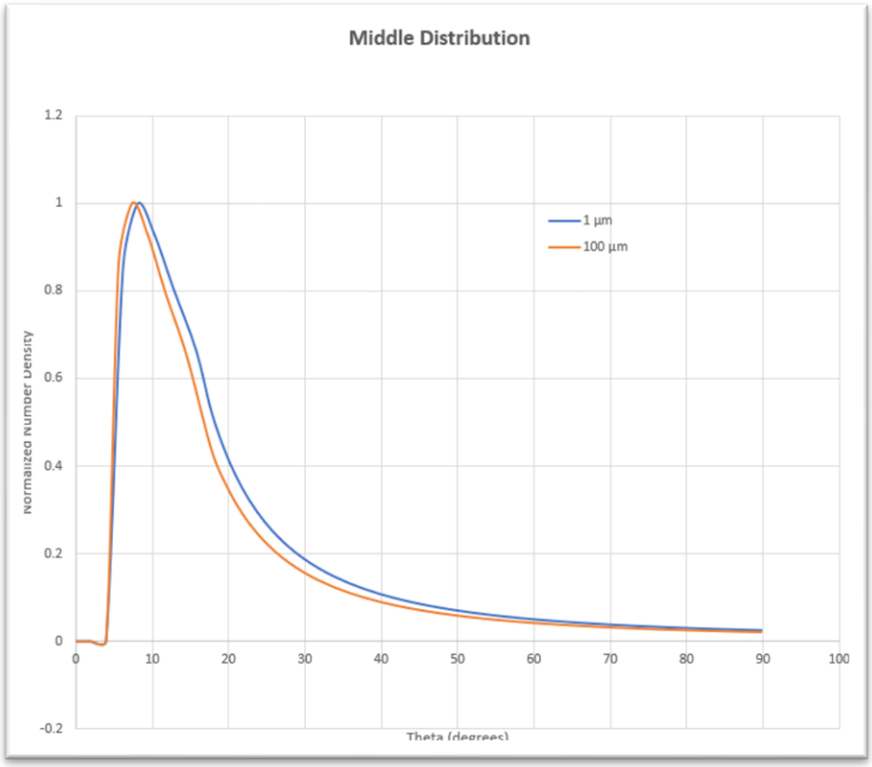

Figure 17: Number density vs angle comparison between 1µm and 100µm diameter particles for the middle distribution case. Unlike the empirical model suggests, the plot is not centered at the centerline meaning this is an unlikely distribution of unburnt droplet concentration.

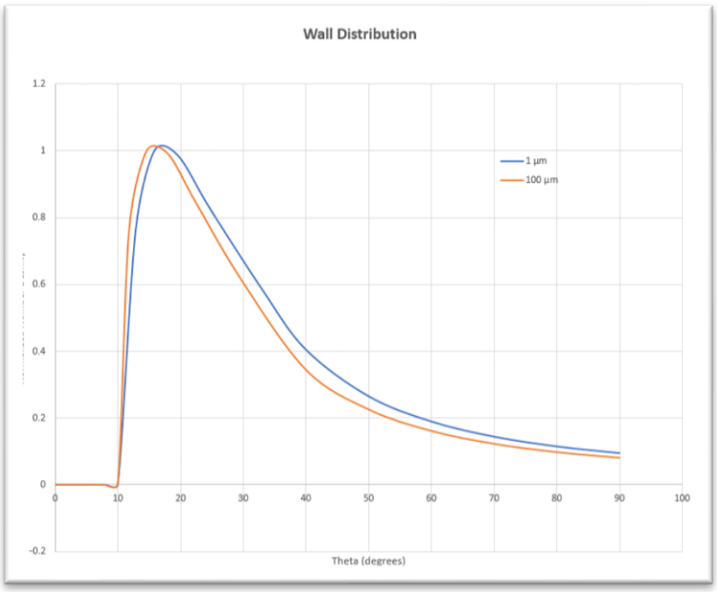

Figure 18: Number density vs angle comparison between 1µm and 100µm diameter particles for the wall distribution case. Unlike the empirical model suggests, the plot is not centered at the centerline meaning this is an unlikely distribution of unburnt droplet concentration.

For all 4 cases the trend observed was that the smaller particles had a larger droplet angular distribution which agrees with findings by Larin in Figure 6 [3]. From Figure 15 the effect particle size has on the number desnity is not substantial which is contrary to what was expected and requires further study.

4. Conclusion

It can be concluded that the most probable particle concentration in the nozzle is either a uniform distribution along the entire inlet of the nozzle or at the center of the nozzle inlet. The number density flux reults correlate with the gaussian form of the Larin equation and both dsitributions are centered along the centerline which also correlates with Larin's equation.

The discrepency in figure 8 between the graphing of the Larin equation and Alred's results points to a difference in the equations being used, more specifically in the equation used for calcualating σ which depends on the limitting angle of the particles in the plume.

4.1 Future Works

Currently no model exists (that the authors are aware of) with the correlation between the limitting angle and particle diameter for the R-4D-11 490N thruster. There is an equation that relates limitting angle and particle diameter for the MBB 10 N thruster [3]. Using the StarCCM+ simulation, it was possible to obtain the limitting angle for different particle size.

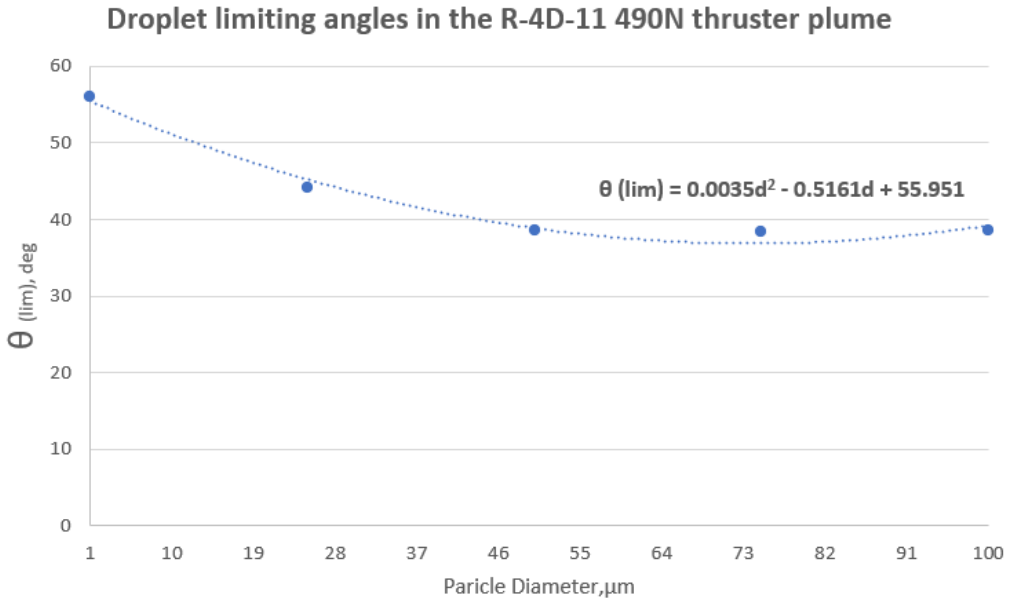

Figure 19 Limiting angle for different particle diameters

Currently, as seen on figure 8, the plots for number density flux as a function of diameter for different angles from the Alred paper do not match with those replicated using the Larin equation. The Larin paper uses an equation crated from the MBB 10 N thruster data for the calcualtion of σ [3].

$$\sigma = \frac{\frac{12}{(d/d_{min})^{0.55}} + 16.7}{\sqrt{12 * ln10}} \tag{12}$$

The number desnity calculation above from the R-4D-11 490N thruster simulation gives a new θ_{lim} and therfore a new equation for calulating σ.

$$\sigma = \frac{0.0035d^2 - 0.5161d + 55.951}{\sqrt{12 * ln10}} \tag{13}$$

For future works it may be possible to get graphs for the number density flux as a function of diameter at different angles that more closely follow the trends seen on the Alred paper using this new value for σ.

The next components of the internship will entail increasing the complexity of the CFD simulations in Star-CCM+:

- Incorporate multicomponent non-reactive exhaust gas in the chamber and change the inflow temperature and pressure to those calulcated using the chemical equations [7]
- Incorporate reacting multicomponent gas following 4 stage combsution [8]
- Incorporate multiphase with reacting gases, liquid active lagrangian droplets, and evaporation model [9]

References

[1] G. DETTLEFF, "PLUME FLOW AND PLUME IMPINGEMENT IN SPACE TECHNOLOGY," *Prog. Aerospace Sci,* vol. 28, 1991.

[2] G. Cai, "A Review of Research on the Vacuum Plume," *Aerospace,* vol. 9, p. 706, 2022.

[3] M. Larin, "Modeling unburned propellant droplet distribution and velocities in plumes of small bipropellant thrusters," *35th AIAA Thermophysics Conference,* 2001.

[4] C. Soares, "Improvements in Modeling Thruster Plume Erosion Damage to Spacecraft," *The Boeing Company,* 2015.

[5] C. Soares, "Thruster Plume Induced Contamination Measurements," *The Boeing Company,* 2002.

[6] J. Alred, "MODELING OF THRUSTER PLUME INDUCED EROSION," *9th International Symposium on Materials in a Space Environment,* 2003.

[7] K. H. Lee, "Plume influence analysis," *PLoS ONE,* 2018.

[8] K. H. Lee, "Numerical simulation on thermal and mass diffusion of MMH–NTO bipropellant thruster plume flow using global kinetic reaction model," *Seoul,,* 2019.

[9] Lingyun Hou, "Chemical Mechanism of MMH/NTO and Simulation in a Small Liquid Rocket," *Combustion Science and Technology,* 2018.